REPORT

De Novo Mutations in *SLC25A24* Cause a Disorder Characterized by Early Aging, Bone Dysplasia, Characteristic Face, and Early Demise

Karin Writzl,[1,*] Ales Maver,[1] Lidija Kovačič,[2] Paula Martinez-Valero,[3,4,5] Laura Contreras,[3,4,5] Jorgina Satrustegui,[3,4,5] Marco Castori,[6] Laurence Faivre,[7,8] Pablo Lapunzina,[9] André B.P. van Kuilenburg,[10] Slobodanka Radović,[11] Christel Thauvin-Robinet,[7,8] Borut Peterlin,[1] Araceli del Arco,[4,5,12] and Raoul C. Hennekam[13]

A series of simplex cases have been reported under various diagnoses sharing early aging, especially evident in congenitally decreased subcutaneous fat tissue and sparse hair, bone dysplasia of the skull and fingers, a distinctive facial gestalt, and prenatal and postnatal growth retardation. For historical reasons, we suggest naming the entity Fontaine syndrome. Exome sequencing of four unrelated affected individuals showed that all carried the *de novo* missense variant c.649C>T (p.Arg217Cys) or c.650G>A (p.Arg217His) in *SLC25A24*, a solute carrier 25 family member coding for calcium-binding mitochondrial carrier protein (SCaMC-1, also known as SLC25A24). SLC25A24 allows an electro-neutral and reversible exchange of ATP-Mg and phosphate between the cytosol and mitochondria, which is required for maintaining optimal adenine nucleotide levels in the mitochondrial matrix. Molecular dynamic simulation studies predict that p.Arg217Cys and p.Arg217His narrow the substrate cavity of the protein and disrupt transporter dynamics. *SLC25A24*-mutant fibroblasts and cells expressing p.Arg217Cys or p.Arg217His variants showed altered mitochondrial morphology, a decreased proliferation rate, increased mitochondrial membrane potential, and decreased ATP-linked mitochondrial oxygen consumption. The results suggest that the *SLC25A24* mutations lead to impaired mitochondrial ATP synthesis and cause hyperpolarization and increased proton leak in association with an impaired energy metabolism. Our findings identify *SLC25A24* mutations affecting codon 217 as the underlying genetic cause of human progeroid Fontaine syndrome.

Human progeroid syndromes encompass a group of genetic disorders that share clinical features of accelerating aging and are known to arise through different pathogenic mechanisms. Alterations in components of the nuclear envelope are the cause of Hutchinson-Gilford progeria syndrome (HGPS [MIM: 176670]),[1,2] whereas impaired DNA-repair mechanisms cause Werner syndrome (MIM: 277700) and Cockayne syndrome (CS [MIM: 216400]).[3,4] In some progeroid syndromes (e.g., Penttinen-type premature aging syndrome (MIM: 601812),[5] the cause is known but the mechanism is incompletely understood, whereas in others both the etiology and pathogenesis remain unknown. Fontaine syndrome is an infrequently described human progeroid syndrome characterized by prenatal and postnatal growth retardation, decreased subcutaneous fat tissue, sparse hair, a triangular face, a widely open anterior fontanel, craniosynostosis (in some), a convex and broad nasal ridge, micrognathia, small distal phalanges of the fingers and toes, and early death (in most).[6–13] It was first reported by Fontaine et al. in 1977,[6] so we suggest naming the entity Fontaine syndrome. It is likely to be the same entity as described by Petty et al.[7] (Petty-type congenital progeroid syndrome [MIM: 612289]). Here, we show that recurrent mutations in *SLC25A24* (solute carrier family 25 member 24 [MIM: 608744]), encoding one of the mitochondrial ATP-Mg/Pi carriers, are responsible for Fontaine syndrome in four deceased individuals.

The parents of all affected individuals provided written informed consent, and the study was approved by the Republic of Slovenia National Medical Ethics Committee (012-78/2015-2, KME 76/07/15). Individuals originated from Slovenia, France, Spain, and Italy.

Individual 1 is described in detail in the Supplemental Note, and individuals 2,[9] 3,[8] and 4[12] have been published before. All presented with prenatal and postnatal growth retardation; an aged appearance characterized by decreased subcutaneous fat, wrinkled skin, and prominent veins; a large anterior fontanel, an abnormal scalp hair pattern, similar facial dysmorphisms (e.g., triangular face, convex nasal ridge, and low-set ears), and small nails and

[1]Clinical Institute of Medical Genetics, University Medical Centre, 1000 Ljubljana, Slovenia; [2]Novartis Ireland Ltd., Novartis, Vista Building, Elm Business Park, D04A9N6 Dublin 4, Ireland; [3]Departamento de Biología Molecular, Centro de Biología Molecular Severo Ochoa, Universidad Autónoma de Madrid and Consejo Superior de Investigaciones Científicas, 28049 Madrid, Spain; [4]Instituto de Investigación Sanitaria Fundación Jiménez Diaz, 28049 Madrid, Spain; [5]Centro de Investigación Biomédica en Red de Enfermedades Raras, Instituto de Salud Carlos III, 28049 Madrid, Spain; [6]Division of Medical Genetics, Casa Sollievo della Sofferenza, Istituto di Ricovero e Cura a Carattere Scientifico, 71013 San Giovanni Rotondo, Foggia, Italy; [7]Centre de Référence Maladies Rares "cAnomalies du Développement et Syndromes Malformatifsc," Centre de Génétique, FHU-TRANSLAD, Hôpital d'Enfants, Centre Hospitalier Universitaire Dijon Bourgogne, 21079 Dijon, France; [8]UMR 1231, Génétique des Anomalies du Développement, INSERM, Université de Bourgogne Franche-Comté, 21079 Dijon, France; [9]Instituto de Genética Médica y Molecular-IdiPAZ, Hospital Universitario La Paz, Centro de Investigación Biomédica en Red de Enfermedades Raras, 261-28046 Madrid, Spain; [10]Laboratory Genetic Metabolic Diseases, Academic Medical Center, University of Amsterdam, 1105 AZ Amsterdam, the Netherlands; [11]IGA Technology Services Srl., 33100 Udine, Italy; [12]Facultad de Ciencias Ambientales y Bioquímica, Centro Regional de Investigaciones Biomédicas, Universidad de Castilla la Mancha, 45071-Toledo, Spain; [13]Department of Pediatrics, Academic Medical Center, University of Amsterdam, 1105AZ Amsterdam, the Netherlands
*Correspondence: karinwritzl@gmail.com
https://doi.org/10.1016/j.ajhg.2017.09.017.

distal phalanges, especially on the ulnar and fibular sides. In addition, two individuals had craniosynostosis. All died by the age of 7 months, including two who died on the first day of life. A summary of clinical findings is provided in Table 1, photos are available in Figure 1, and pedigrees can be found in Figure S1.

The four individuals were the only affected individuals in their families, none of the parents were consanguineous, and both sexes were equally affected. Therefore, we hypothesized that the syndrome is caused by a heterozygous *de novo* variant in a single gene and performed exome sequencing in two trios (individuals 1 and 2 and their parents) (Tables S1 and S2). We identified a *de novo* missense variant in *SLC25A24* (c.650G>A [p.Arg217His] [GenBank: NM_013386]) in both individuals and confirmed the variant by Sanger sequencing (Table S3). The DNA sample from individual 3 was isolated from a formalin-fixed paraffin-embedded tissue sample. Because the DNA sample was severely degraded, neither exome sequencing nor Sanger sequencing was feasible; therefore, whole-genome sequencing and a single-base extension assay were performed. Whole-genome sequencing followed by bioinformatic analysis focused on genetic variation in *SLC25A24* demonstrated a *de novo* variant affecting the same amino acid residue (c.649C>T [p.Arg217Cys] [GenBank: NM_013386]). Validation with the single-base extension assay confirmed the variant in heterozygous form (Table S4 and Figure S1). Subsequently, we screened individual 4 by Sanger sequencing and identified the same *de novo* variant as in individuals 1 and 2.

The detected variants c.649C>T and c.650G>A target a single arginine residue (Arg217), are computationally predicted to be damaging (by SIFT, PolyPhen-2, MutationTaster), and are absent from dbSNP 141, the Slovenian exome database, GnomAD, GoNL, and the UK10K database.

SLC25A24, also known as *SCaMC-1* (short calcium-binding mitochondrial carrier isoform 1)[14] or *APC1* (mitochondrial ATP-Mg/P_i carrier isoform 1),[15] is a member of the solute carrier 25 (*SLC25*) family of nuclear genes, which encodes 53 mitochondrial carriers responsible for the transport of nucleotides, metabolites, and cofactors across the mitochondrial inner membrane.[16] *SLC25A24* encodes one of five ATP-Mg/Pi carriers. The main function of ATP-Mg/Pi carriers is the exchange of ATP-Mg or ADP for phosphate across the mitochondrial inner membrane. It is performed in an electro-neutral and reversible way depending on the relative ATP-Mg and phosphate concentration gradients and strictly on extra-mitochondrial Ca^{2+}.[15,17] This way, optimal adenine levels are maintained in the mitochondrial matrix, which is required for effective respiratory activity, metabolism (gluconeogenesis and urea synthesis), mitochondrial protein synthesis and proliferation, and regulation of the Ca^{2+} -mediated mitochondrial permeability transition (mPT).[17,18] Increased mPT can be evident by loss of mitochondrial membrane potential, mitochondrial swelling, efflux of solutes under 1.5 kDa, and cell death; it is the final pathway of cell death in many pathologies,[19] indicating that ATP-Mg/Pi carriers play an important role in cell survival. SLC25A24 carriers are monomers[20] consisting of three tandemly repeated homologous domains, each containing two transmembrane α helices and one conserved mitochondrial carrier family (MCF) signature (Figure 2A). Both N and C termini face the cytosolic side of the inner mitochondrial membrane, and the six α helices form a compact inner mitochondrial transmembrane domain.[27] The N-terminal domain forms a calcium-sensitive regulatory domain.[14,15]

The two presently detected variants target a single arginine residue (Arg217), located just below the m-gate of the carrier (Figure 2). Arg217 is part of the MCF signature P-X-[D/E]-**R**-X-[K/R], which is fully conserved among ATP-Mg/Pi carriers and ADP/ATP carriers (Figure S2), indicating its importance for the function and/or structure of mitochondrial adenine carriers. Further evidence supporting the pathogenicity of the detected variants was found by modeling and molecular dynamics simulation of human SLC25A24 based on the bovine mitochondrial ADP/ATP carrier model (PDB: 1OKC) (Figure 2). This showed that Arg217 is critical for the structural stability of SLC25A24 by maintaining rigid distances between the ends of helices 2 and 3 through four strong hydrogen bonds with three backbone residues. The substitutions at Arg217 were predicted to either abolish these hydrogen bonds completely (p.Arg217Cys) or allow only a single one to form (p.Arg217His) and thereby dramatically alter the structure of the protein. This alteration is expected to narrow the substrate cavity and therefore disturb the entry of nucleoside into the carrier and change the transporter dynamics.

Further studies demonstrated similar amounts of SLC25A24 between skin fibroblasts of affected individual 4 and control fibroblasts, whereas in fibroblasts from an individual with a very small deletion encompassing *SLC25A24*,[28] protein amounts were reduced by 50% (Figure 3A, right). Immunofluorescence staining showed that p.Arg217His localized fully to mitochondria (Figure 3B). Fibroblasts derived from affected individual 4 showed enlarged, swollen mitochondria close to the nucleus (Figure 3B, arrowheads) and abnormal cristae at the electron-microscopy level (Figure 3C), whereas cristae were smaller and less dense in normal, non-swollen mitochondria (Figure 3C).

To examine the effects on mitochondrial morphology, we overexpressed FLAG-tagged full-length SLC25A24 variants p.Arg217His and p.Arg217Cys and wild-type (WT) SLC25A24 in different cell lines. As previously reported,[14] overexpression of WT SLC25A24 did not cause morphological alterations in mitochondria (Figure 3D), but occasional fragmentation and perinuclear clustering was observed (data not shown). Compared with cells transfected with WT SLC25A24, cells transfected with the

Table 1. Clinical Presentation in Four Individuals with Fontaine Syndrome and an *SLC25A24* Mutation

	Individual 1	Individual 2	Individual 3	Individual 4	Summary
SLC25A24 mutation	c.650G>A (p.Arg217His)	c.650G>A (p.Arg217His)	c. 649G>T (p.Arg217Cys)	c.650G>A (p.Arg217His)	NA
Inheritance	*de novo*	*de novo*	*de novo*	*de novo*	4 *de novo*
Sex	male	female	female	male	2 female and 2 male
IUGR	+	+	+	+	4/4
Oligohydramnios	+	+	+	+	4/4
Gestational age (weeks)	34	38	35	32	NA
Birth weight	1,390 g ($<3^{rd}$ percentile)	1,700 g ($<3^{rd}$ percentile)	800 g ($<3^{rd}$ percentile)	866 g ($<3^{rd}$ percentile)	4/4 < 3^{rd} percentile
Postnatal growth (length)	$<0.4^{th}$ percentile	$<0.4^{th}$ percentile	NK	NK	2/2 < 0.4^{th} percentile
Age at death	6 months	7 months	7 hr	20 hr	7 hr to 7 months
Cause of death	pulmonary hypertension	sepsis	respiratory distress	respiratory distress	NA
Clinical Features					
Aged appearance	+	+	+	+	4/4
Decreased subcutaneous fat	+	+	+	+	4/4
Wrinkled skin	+	+	+	+	4/4
Prominent veins	+	+	+	+	4/4
Wide fontanels	+	+	+	+	4/4
Craniosynostosis	+	NK	NK	+	2/2
Abnormal scalp hair pattern	+	+	+	+	4/4
Triangular face	+	+	+	+	4/4
Convex nasal ridge	+	+	+	+	4/4
Micrognathia	+	+	+	−	3/4
Low-set ears	+	+	+	+	4/4
Small distal phalanges	+	+	+	+	4/4
Small nails	+	+	+	+	4/4
Umbilical hernia and/or underdeveloped abdominal muscles	+	+	−	+	3/4
Cryptorchidism	+			+	2/2
Cardiovascular anomalies	BAV, PAH	PDA	−	−	2/4
CNS anomalies	−	NK	−	+[a]	1/3
Radiological Features					
Poor skull ossification	+	+	NK	−	2/3
Craniosynostosis	+	−	NK	+	2/3
Small or absent distal phalanges[b]	+	+	+	+	4/4
Postmortem Examination					
Deficient enchondral ossification	NK	NK	+	NK	1/1
Reduced number of alveoli	+	NK	+	−	2/3
Liver steatosis	+	NK	NK	NK	1/1

Abbreviations are as follows: +, present; −, not present; BAV, bicuspid aortic valve; CNS, central nervous system; IUGR, intrauterine growth restriction; PAH, pulmonary artery hypertension; PDA, persistent ductus arteriosus; NA, not applicable; and NK, not known.
[a]Gyral abnormalities, periventricular heterotopia, and cerebellar underdevelopment.
[b]Especially the ulnar and fibular sides.

Figure 1. Clinical Findings in the Presently Described Individuals with Fontaine Syndrome
(A–H) Facies of individual 1 at ages 3 days (A), 17 days (F), and 4 months (B, front; G, side); individual 2 (C, font; H, side) individual 3 (D); and individual 4 (E) demonstrate the triangular shape of the face, abnormal skull shape due to craniosynostosis in individuals 1 and 4, sparse hair, limited subcutaneous fat, wrinkled skin, broad eyebrows (especially laterally), short nose with broad nasal tip, and low-set ears.
(I–M) Toes of individual 1 (I) and individual 4 (J) and fingers of individual 1 (K and L) and individual 4 (M). Note the small terminal phalanges and small nails, which are more marked on the ulnar and fibular sides.

p.Arg217His or p.Arg217Cys variant showed striking changes of mitochondrial phenotypes. Most of the cells displayed enlarged nuclear-adjacent FLAG-positive structures corresponding to swollen mitochondria that fully matched those labeled with mitochondrial markers such as TOMM20 (Figure 3E), endogenous SLC25A24, MitoTracker, or β-ATPase (data not shown). HeLa cells and COS-7 cells expressing either variant showed abnormally swollen mitochondria similar to those found in the fibroblasts of affected individual 4 (Figure 3D). However, in contrast to mutant fibroblasts from individual 4, the whole mitochondrial network appeared homogenously affected, probably as result of the higher expression levels.

Western blot analysis of HeLa cell lines expressing either the p.Arg217Cys variant or WT SLC25A24 demonstrated that the exogenously expressed proteins reached levels approximately similar to those of endogenous SLC25A24, representing a suitable tool for analyzing the functional effects of the *SLC25A24* mutation (Figure 4A). However, the two exogenously expressed proteins did not reach the same levels. Notably, p.Arg217Cys-expressing clones showed lower protein levels than those expressing WT SLC25A24 (Figure 4A) and were obtained at a lower frequency, suggesting a detrimental effect of the p.Arg217Cys variant on cellular viability. Indeed, the xCELLigence biosensor system showed that the proliferative ability of cells harboring the p.Arg217Cys variant was lower than that of cells harboring WT SLC25A24 (Figures 4B and 4C). The difference in growth rate and the morphology of mutant mitochondria suggest a functional impairment of mitochondria.

Studies of mitochondrial membrane potential ($\Delta\psi$) by tetramethylrhodamine methylester (TMRM) microfluorimetry in the non-quench mode[18,29] and of the basal oxygen consumption rate (OCR) with the Extracellular Flux Analyzer (Seahorse) showed that mitochondrial function was altered: calibrated basal membrane potential was

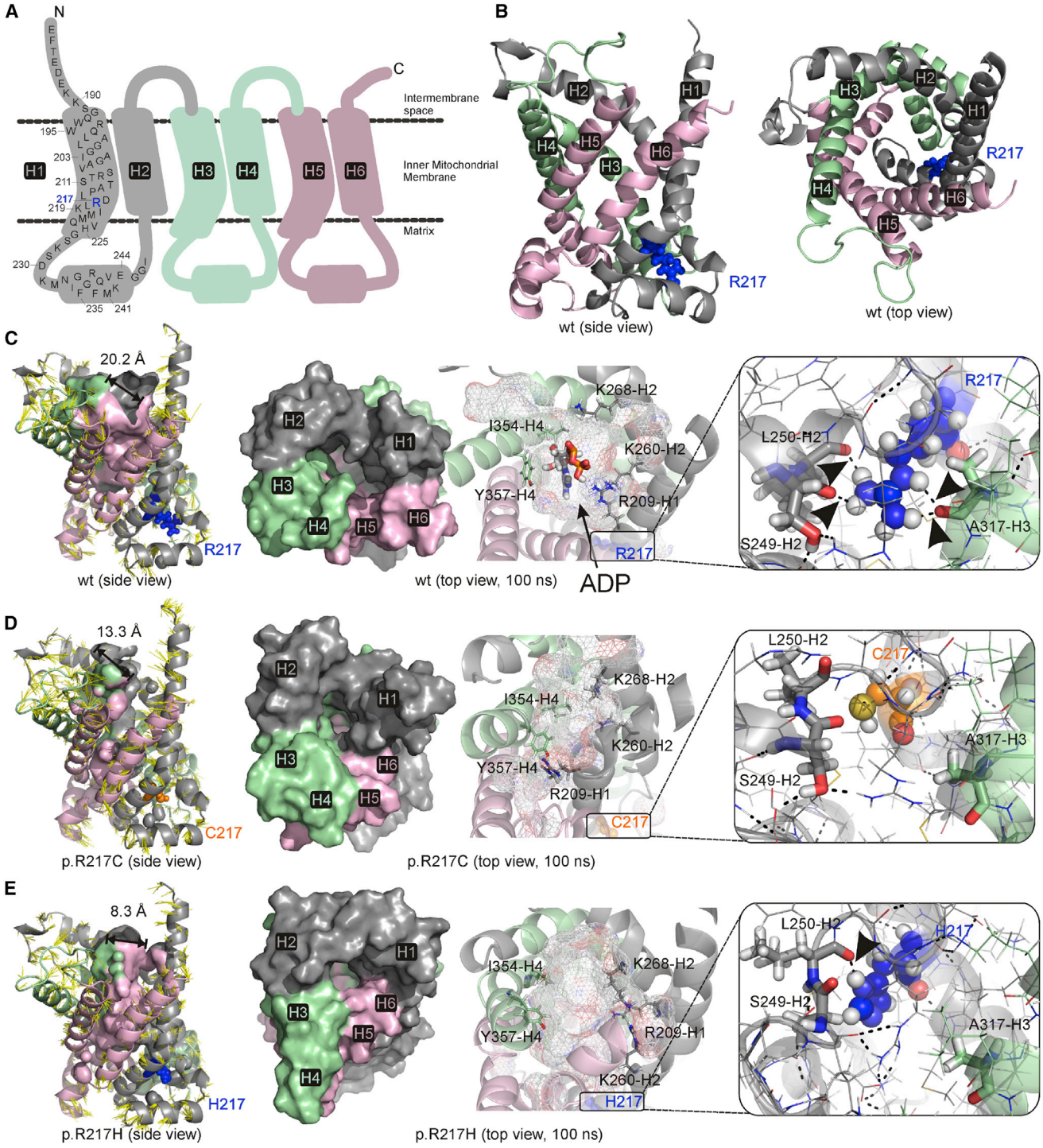

Figure 2. ***In Silico*** **Modeling Predicts that p.Arg217Cys or p.Arg27His Causes Significant Structural Changes within the SLC25A24 Transmembrane Domain**

(A) Topologic model of the transmembrane domain of SLC25A24 depicts amino acids 183–247, including Arg217 (dark blue). The numbering of the transmembrane α helixes and the coloring of the three repeat units (gray, light green, and light pink) are consistent throughout the figure.

(B) 3D model of amino acids 188–469 of WT SLC25A24 (shown in side and top views) depicts Arg217 in spherical presentation. The SLC25A24 transmembrane domain consists of six transmembrane α helixes, tilted in the orthogonal direction in a deep-cone-shaped barrel, whose structure is dynamic to allow for efficient substrate transport, as previously described for a similar transporter.[21]

(C–E) Left: molecular dynamic simulation studies of WT (C), p.Arg217Cys (D), and p.Arg217His (E) SLC25A24 (amino acids 188–469) followed for 1, 2, 4, 6, 8, 10, 12, 14, 16, 18, 20, 24, 28, 40, and 100 ns. A monomer without ADP was used as a starting unit for each simulation, which included movements from 0 to 100 ns,[22,23] and the ADP structure was than superimposed. All structures were evaluated in PyMol. Each yellow line represents the movement of a single backbone amino acid from the WT. The distance between Gln284 and Tyr461, indicating the center 100 ns simulated structure, is provided in Ångstroms and shows that the substrate cavity narrowed

(legend continued on next page)

higher in p.Arg217Cys-expressing HeLa cell lines and in fibroblasts from individual 4 than in control cells (Figures 4D and 4E). Basal and maximal uncoupled OCRs in the WT and p.Arg217Cys proteins were not significantly different (data not shown), but the contribution of ATP synthesis to basal mitochondrial respiration was clearly lower in the p.Arg217Cys variant than in WT SLC25A24 (Figures 4F and 4G). These results indicate that mitochondrial hyperpolarization is associated with impaired ATP synthesis by mutant mitochondria, in agreement with the known effects of oxidative phosphorylation (OXPHOS) inhibition on the proton electrochemical potential.[35] However, no significant decrease in basal amounts of cytosolic or mitochondrial ATP was detected by the GO-ATeams FRET (Förster resonance energy transfer) probes directed to mitochondria (Figure 4H) or the cytosol (Figure 4I). This is perhaps not surprising given that most tumor cells rely on glycolytic ATP production.[36] To test whether inhibition of the oligomycin-sensitive OCR is due to a decrease in ATP demand in mutant cells, we studied the amount of mitochondrial ATP upon inhibition of mitochondrial ATP synthesis with oligomycin. This caused a rapid decline in the amount of mitochondrial ATP, which was more pronounced in mutant than in control cells (Figure 4J), indicating that ATP demand was increased in mutant cells. The results strengthened the notion that the primary effect of the mutation is not decreased ATP demand but decreased mitochondrial ATP production, which increases the membrane potential, and a subsequent increase in proton leak.

Together, our results demonstrate that Fontaine syndrome mutations in *SLC25A24* clearly affect mitochondrial morphology and suggest an impact on OXPHOS via decreased ATP synthesis and increased $\Delta\psi$. This creates conditions under which cell proliferation is hampered. The mechanisms through which these mutations affect mitochondrial morphology and ATP synthesis could be related to structural modification of the ATP-Mg/Pi carrier and its interactions with other mitochondrial membrane proteins.

SLC25A24 has been suggested to play an important role in modulating cell-death pathways by influencing the opening of the mPT pore through regulation of the calcium-buffering capacity of mitochondria and regulation of the total mitochondrial adenine content.[18] SLC25A24 is overexpressed in a wide range of tumors, cancer cell lines, and highly proliferative immortalized cells, initiating a strong cytoprotective effect.[18] Knockdown of *SLC25A24* renders cells more susceptible to mPT-dependent cell death, triggered by oxidative stress and Ca^{2+} overload.[18] Heterozygous deletion of *SLC25A24* in an individual with a 1p13.3p21.3 microdeletion[28] halves the amount of SLC25A24 in fibroblasts but has no effect on mitochondrial morphology and does not manifest with an early aging phenotype. Individuals with Fontaine syndrome show normal amounts of SLC25A24 in fibroblasts but marked changes in mitochondrial morphology and function, suggesting a pathological gain of function of the mutated SLC25A24.

Mitochondrial dysfunction has been previously reported in several premature-aging syndromes caused either by alterations in components of the nuclear envelope, such as in laminopathies HGPS[37] and mandibuloacral dysplasia with type B lipodystrophy (MADB [MIM: 608612]),[38] or by impaired DNA repair, such as in CS,[39] ataxia-telangiectasia (AT [MIM: 208900]),[40] and xeroderma pigmentosum, complementation group A (XPA [MIM: 278700]).[41] The underlying molecular mechanisms for the premature-aging phenotypes are far from clear. In HGPS cells, defective OXPHOS, increased reactive oxygen species, and elevated oxidative stress have been reported.[37] For MADB, an entity that shares several manifestations with Fontaine syndrome, studies on human ZMPSTE24-knockdown fibroblasts showed changes in mitochondrial potential, reduced mitochondrial respiration, and decreased cell proliferation.[42] Cells of individuals with CS, AT, and XPA show comparable mitochondrial alterations consisting of lower mitophagy, increased mitochondrial content, higher membrane potential, higher basal OCR, and higher ATP consumption as a result of the activation of the DNA-damage response to persistent nuclear DNA damage.[43] Secondary mitochondrial dysfunction could have an important role in the pathogenesis of the majority of progeroid syndromes, but here we present evidence that Fontaine syndrome is caused by a nuclear-encoded mitochondrial

from 20 Å (WT) to 13 Å (p.Arg217Cys) to 8 Å (p.Arg217His). Middle left: the surface presentation of the 100 ns simulated structure of WT, p.Arg217Cys, and p.Arg217His SLC25A24 (amino acids 188–469) shows the change in shape of the substrate cavity from circular to ellipsoid. Middle right: enlarged entrance region of substrate cavity in SLC25A24 (amino acids 188–469). The main amino acids (Arg209, Lys260, Lys268, Ili354, and Tyr357) needed for transport and conformational change of the cavity during transport are shown in stick representation (in the WT, hydrogen bonds are shown as dashed black lines). ADP is indicated in red (acidic), yellow (phosphor), and dark gray (carbon) sticks. In the open state (WT, C), ADP can bind to the indicated amino acids, which releases energy, allowing the cavity to close and open at the other side. *SLC25A24* mutations affecting Arg217 (D and E) deform the entrance and inhibit bonding to the indicated amino acids, inhibiting conformational changes of the cavity and thus transport. Right: further enlargement of Arg217 and its interaction network. Arrowheads indicate side-chain interactions between Arg217 and the backbone amino acids of helices 2 and 3. Modeling was performed with the program Modeler 9v14[24] and default parameters for the protocols "allHmodel2" (for inclusion of hydrogen atoms) and "HETATM" (for inclusion of ADP) and a refinement protocol allowing up to 50 variable iterations with five repeats. Putative structural changes caused by mutations were simulated with a NAMD 2.11 program[25] plug-in in Visual Molecular Dynamics v.1.9.2.[26] Model p.Met221Ile was added as a control for the molecular dynamic simulation protocol because this variant was reported in the homozygous state in a healthy individual (according to the ExAC Browser) and was computationally predicted to be benign (by SIFT and MutationTaster). High similarity was observed among the modeled WT structure, p.Met221Ile, and the initial template (PDB: 1OKC)[27] in terms of repeat-channel depth and width, nucleotide binding cavity, and ADP binding residues.

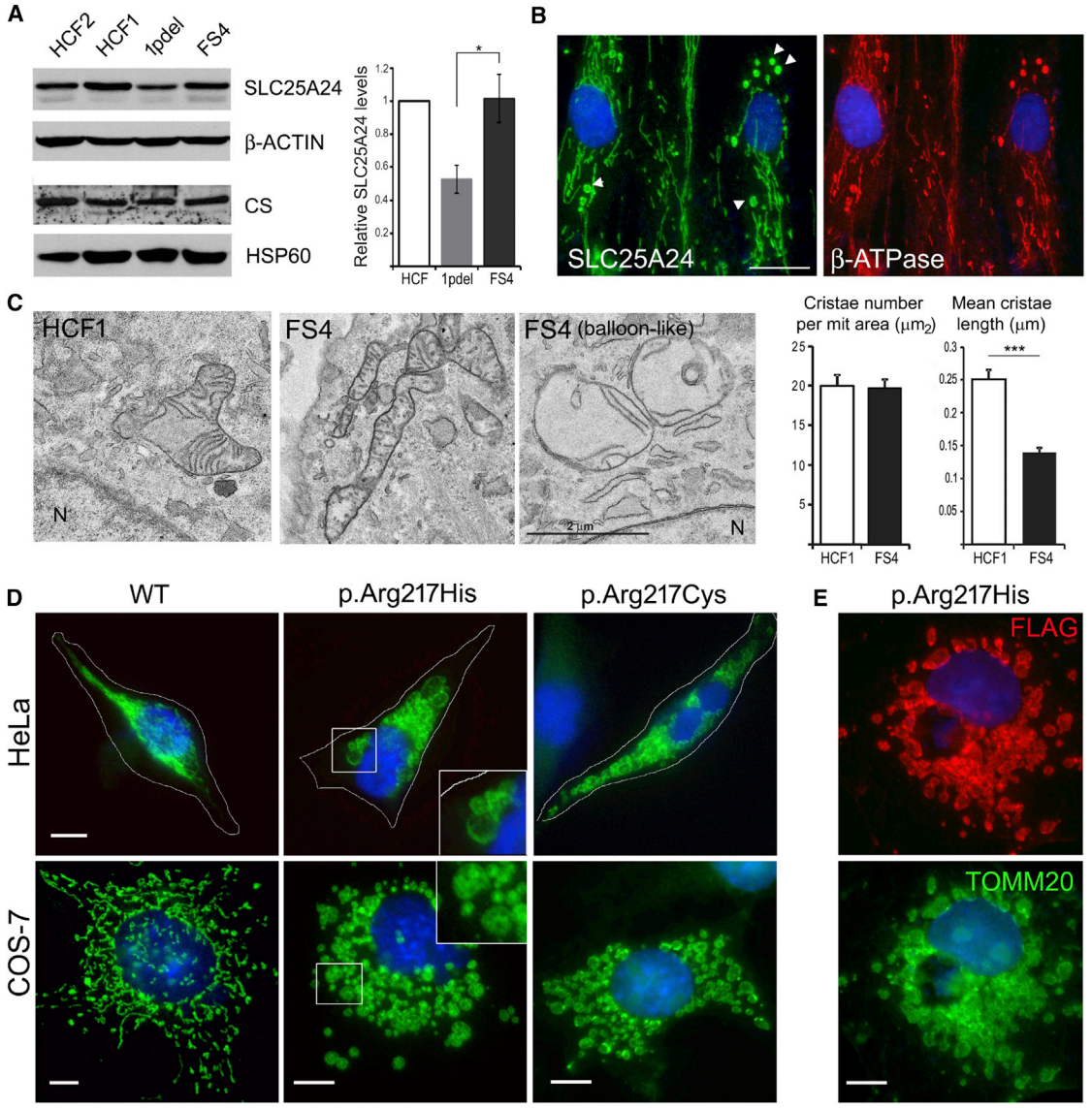

Figure 3. SLC25A24 p.Arg217His and p.Arg217Cys Localize to Mitochondria and Affect Mitochondrial Morphology

(A) Representative western blot and quantification of SLC25A24 in cell lysates of fibroblasts harboring the p.Arg217His variant (from individual 4 [FS4]), a fibroblast cell line containing a heterozygous microdeletion encompassing *SLC25A24* (1pdel),[28] and healthy control fibroblasts (HCF1 [NHDF-Neonatal. CC-2509, Lonza] and HCF2 [obtained from a normal newborn skin biopsy]). Total protein extraction and western blot analysis were performed according to standard procedures. A polyclonal antibody raised against human SLC25A24 at a 1:5,000 dilution was used.[14] Blots were stripped and re-probed with monoclonal anti-β-actin (Sigma; 1:10,000 dilution) as an internal loading control. Parallel blots were incubated with anti-citrate synthase (CS) (Sigma; 1:1,000 dilution) and anti-HSP60 (Stressgene; 1:10,000 dilution) as mitochondrial controls. Peroxidase-coupled horse anti-mouse and goat anti-rabbit (Vector Laboratories) were used as secondary antibodies at a 1:10,000 dilution. Proteins were detected with ECL (Amersham Biosciences). Films were scanned with the GS-900 calibrated densitometer (Bio-Rad). Right: densitometry analyses of the amount of SLC25A24 in fibroblasts from individual 4; values are expressed as the ratio of SLC25A24 to β-actin and are normalized with respect to HCF values on each experimental day. No significant differences were observed between fibroblasts from FS4 and control fibroblasts. Data represent the mean ± SEM of three independent experiments.

(B) Immunofluorescence analysis of SLC25A24 in FS4 fibroblasts with polyclonal anti-SLC25A24 antibody (1:400 dilution).[14] Alexa Fluor 488 goat anti-rabbit (Invitrogene; 1:400 dilution) and Cy3-conjugated goat-anti-mouse (Jackson InmunoResearch; 1:1,000 dilution) were used as secondary antibodies. SLC25A24 signals (green) matched those of the mitochondrial marker β-ATPase (red) (Abcam; 1:200 dilution), indicative of an exclusive mitochondrial location of the p.Arg217His variant. Arrowheads indicate swollen balloon-like mitochondria observed in FS4 fibroblasts. Scale bar, 20 μm.

(C) Transmission electron microscopy of FS4 and control (HCF1) fibroblasts. Cells were fixed to the culture plate, and ultrathin sections oriented parallel to the cell base were processed. Mitochondria and cristae were identified manually from high-resolution images, and the mitochondrial area and number and length of cristae were determined with ImageJ software. Representative high-magnification images of mitochondria from each fibroblast are shown. A representative image of swollen mitochondria (balloon-like) from FS4 fibroblasts is also shown. Morphometric analyses were performed from randomly selected mitochondria obtained from two independent experiments (100 for FS4 and 135 for HCF1). Mitochondria with balloon-like morphology were excluded. Data represent the mean ± SEM.

(legend continued on next page)

protein alteration causing a primary mitochondrial dysfunction.

A wide range of human disorders have been associated with alterations of mitochondrial carriers of the SLC25 family.[44] The phenotypes have been characterized in general by exercise intolerance, lactic acidosis, cardiomyopathy, myopathy, neuropathy, epilepsy, and microcephaly.[21] These disorders are all autosomal recessive, except for *SLC25A4*-related disorders, which are inherited either autosomal-recessively (autosomal-recessive, cardiomyopathic-type mitochondrial DNA depletion syndrome 12B [MIM: 615418])[45] or autosomal-dominantly (autosomal-dominant, cardiomyopathic-type mitochondrial DNA depletion syndrome 12A [MIM: 617184][46] and autosomal-dominant progressive external ophthalmoplegia with mitochondrial DNA deletions 2 [MIM: 609283]).[47] Mutations in *SLC25A4*, which encodes a mitochondrial ADP/ATP carrier, cause mtDNA instability through a currently unknown mechanism.[46,47] Additionally, increased mtDNA point mutations and deletions,[48] mtDNA replication arrest,[49] and abnormalities of stem cell renewal[50] have been reported in POLG mutator mice with a premature-aging phenotype. Given that the disease phenotype of Fontaine syndrome could be a consequence of mtDNA instability, we performed a search for *de novo* point mutations and structural variants in mtDNA of two probands and found no evidence of an increase in the rate of *de novo* mtDNA mutation events (Table S2).

None of the five isoforms of the highly conserved mitochondrial ATP-Mg/Pi carrier subfamily has been associated with a congenital disorder in humans, which has been attributed to their redundancy and overlapping expression patterns.[51] Human SCaMC mRNAs are ubiquitously present, and more than one isoform has been detected is several human tissues, such as the brain, lung, kidney, heart, skeletal muscle, or heart.[14,15] Of note, in mice, differences in expression of the isoforms at the protein level have been reported; for example, *Slc25a24* is mainly expressed in the small intestine, lung, and colon, and *Slc25a23* (*SCaMC-3*) is exclusively expressed in the liver and brain.[52] Furthermore, studies on *SCaMC*-knockout mice have shown different phenotypes,[53,54] suggesting a specific role of different *SCaMC* isoforms. An obesity-resistant phenotype has been reported in the *Slc25a24*-knockout mouse model.[55] Moreover, SLC25A24 has an important role in mouse fat metabolism and could be critical for adipocyte differentiation: mouse *Slc25a24* is predominantly expressed in white adipose tissue, *Slc25a24* expression is increased in adipose tissue after mice are fed a high-fat diet, and adipocyte differentiation is inhibited in *Slc25a24*-knockout adipose tissue. In humans, it has been suggested that the amount of SLC25A24 might affect body fat percentage and body mass index.[55] This could be related to the pathogenesis of lipodystrophy in individuals with Fontaine syndrome.

In the accompanying article in this issue of *The American Journal of Human Genetics*,[56] Ehmke et al. report the same c.650G>A and 649C>T *SLC25A24* mutations as those found in our individuals, but their phenotype fits Gorlin-Chaudhry-Moss syndrome (GCMS [MIM: 233500]). The phenotypes of the two entities resemble one another on important characteristics such as growth retardation, craniosynostosis, sparse hair, reduced subcutaneous fat, and small distal phalanges. Their differences include some facial characteristics (shape of the nasal ridge, eye size, and chin size), genital development, and especially the fact that Fontaine syndrome leads to early demise and GCMS is accompanied by an apparently normal lifespan. At present, there is no explanation for these differences, but we hypothesize that variations in function of other genes involved in mitochondrial functioning, other genetic and epigenetic influences, and environmental influences might play a role.

In conclusion, we have identified recurrent missense *SLC25A24* mutations affecting codon 217 as the underlying genetic cause of Fontaine syndrome, a condition characterized by congenitally decreased subcutaneous fat tissue, sparse hair, bone dysplasia in the fingers and skull, a distinctive facial gestalt, and prenatal and postnatal growth retardation. *SLC25A24*-mutant fibroblasts and cells expressing p.Arg217Cys or p.Arg217His SLC25A24 showed altered mitochondrial morphology. Additionally, a slower proliferation rate, an increase in mitochondrial membrane potential, and a decrease in mitochondrial oxygen consumption linked to ATP synthesis were detected. We speculate that *SLC25A24* mutations affecting codon 217 impair mitochondrial ATP synthesis and cause hyperpolarization

(A–C) The average length of cristae appeared significantly smaller in FS4 than in HCF1 mitochondria, but no difference in cristae number was observed. In (A) and (C), the statistical significance of differences between the cell lines was analyzed by two-tailed, two-sample Student's t tests (*$p < 0.01$, ***$p < 0.001$).
(D) Transiently transfected HeLa and COS-7 cells overexpressing p.Arg217His and p.Arg217Cys variants showed altered mitochondrial morphology. Site-directed mutagenesis of SLC25A24 to generate the p.Arg217Cys and p.Arg217His variants was performed by overlap extension PCR using a full-length SLC25A24 open reading frame tagged with FLAG epitope at the carboxyl end as a template as previously described.[14] Then, the p.Arg217Cys and p.Arg217His variants were subcloned into the eukaryotic expression vector pCAGGS. Intracellular distribution of WT, p.Arg217His, and p.Arg217Cys SLC25A24 overexpressed in HeLa and COS-7 cells was determined 48 hr after transfection by an immunofluorescence assay using anti-FLAG antibodies (Sigma; 1:200 dilution). Representative HeLa and COS-7 FLAG-positive cells overexpressing WT, p.Arg217His, and p.Arg217Cys proteins are shown. Cell nuclei were stained with DAPI (scale bars, 10 μm; inset, 200× magnification). Note the swollen morphology shown by mitochondria overexpressing SLC25A24 mutant variants, in contrast to the typical tubular mitochondrial network found in the overexpressing WT SLC25A24 cells.
(E) In COS-7 cells overexpressing p.Arg217His, FLAG-positive structures entirely matched those corresponding to the mitochondrial marker TOMM20 (Fitzgerald; 1:200 dilution). Cell nuclei were marked with DAPI. Scale bar, 10 μm.

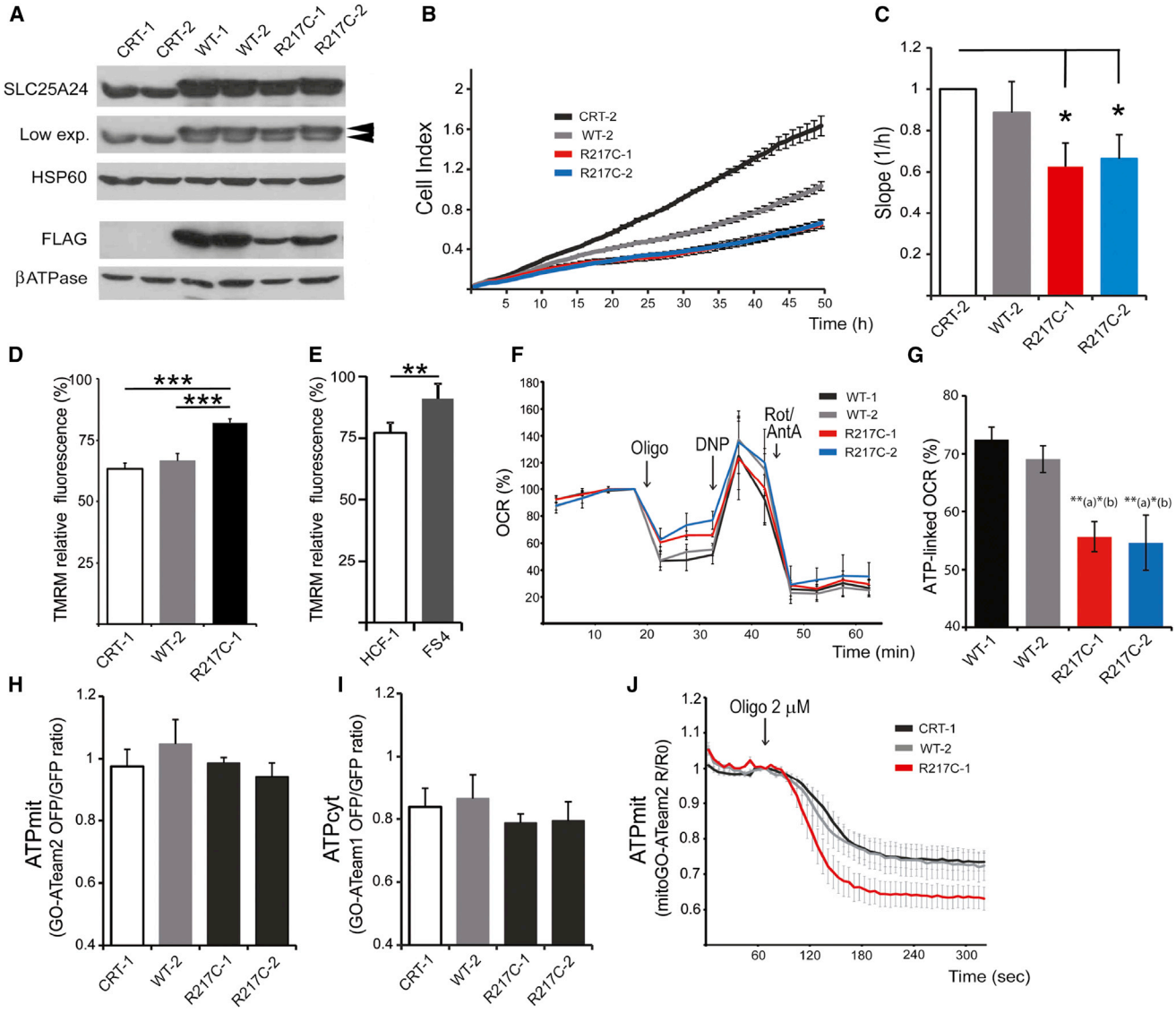

Figure 4. Heterologous Expression of SLC25A24 p.Arg217Cys in HeLa Cells Lowers Cell Proliferation and ATP-Linked Respiration and Increases the Mitochondrial Membrane Potential

For stable expression in HeLa cells, FLAG-tagged WT and p.Arg217Cys (R217C) SLC25A24 were subcloned into a bicistronic pIRES2puro vector. After transfection, clones were selected after the addition of 1 μg/mL puromycin (Sigma).

(A) Western blot analysis of SLC25A24 levels in total protein extracts from HeLa cell lines stably expressing empty vector (pIRES2puro; CRT-1 and CRT-2) or FLAG-tagged WT (WT-1 and WT-2) and p.Arg217Cys (R217C-1 and R217C-2) SLC25A24. Parallel membranes were incubated with specific antibodies against SLC25A24 and FLAG epitope and re-probed with anti-HSP60 and anti- β -ATPase antibodies, respectively, as mitochondrial loading controls under the conditions described in Figure 3A. All cells overexpressing FLAG-tagged SLC25A24 (WT-1, WT-2, R217C-1, and R217C-2) had larger SLC25A24 bands than the controls (CRT-1 and CRT-2), and the bands appeared as doublets; the upper one corresponded to the overexpressed protein, which increased in size as a result of the FLAG epitope. Staining with anti-FLAG allowed distinction between endogenous protein (not stained with anti-FLAG) and overexpressed proteins. From the intensity of these FLAG bands, the mutants (R217C-1 and R217C-2) reached lower levels than the WT proteins (WT-1 and WT-2) (lower intensity in the anti-FLAG staining).

(B and C) p.Arg217Cys SLC25A24 reduced the HeLa proliferation rate. HeLa cells expressing empty vector (CRT-2), WT SLC25A24 (WT-2), and p.Arg217Cys SLC25A24 (R217C-1 and R217C-2) were seeded at a density of 5,000 cells/well in xCELLigence plates, and the cell index (showing the cell proliferation) was monitored with a Real-Time Cell Analyzer DP instrument (Roche). The impedance signals were recorded every 15 min over a period of up to 60 hr. The cell index and slope were calculated automatically by the RTCA Software Package 1.2 of the RTCA system. (B) The cell index was lower in HeLa cells expressing p.Arg217Cys than in HeLa cells expressing the WT or empty vector. (C) The slope (which represents the rate of change of the cell index) was calculated from 2 to 60 hr and normalized with respect to CRT-2 control cells. HeLa cells expressing p.Arg217Cys exhibited a lower cell-proliferation rate than control cells (*$p < 0.05$, paired t test). The results represent the mean ± SEM from three independent experiments from at least four wells per cell line.

(D and E) Mutant SLC25A24 increased the mitochondrial membrane potential. Basal mitochondrial membrane potential, $\Delta\psi$, in HeLa stable lines CRT-1, WT-2, and R217C-1 (n = 85–156) (D) and human fibroblasts HCF1 and FS4 (n = 15–76) (E) was measured by TMRM microfluorimetry[18,29] in the non-quench mode (5 nM, 30 min load into cells) with 500–540 nm excitation and 590–650 nm emission filter settings. Cells were identified as regions of interest, and fluorescence at the nucleus was taken as background. For calculation of the

(legend continued on next page)

and increased proton leak in association with altered energy metabolism. Further research will be needed to decipher the underlying mechanism.

Accession Numbers

The accession numbers for the c.650G>A and c.649C>T variants reported in this paper are ClinVar: SCV000320993 and SCV000320994.

Supplemental Data

Supplemental Data include a Supplemental Note, two figures, and four tables and can be found with this article online at https://doi.org/10.1016/j.ajhg.2017.09.017.

Acknowledgments

We are pleased to thank the families for their generous cooperation. This study was financially supported by grants from the Spanish Ministry of Economy and Competiveness (SAF2014-56929-R to J.S.), Ramón Areces Foundation (to the Centro de Biología Molecular Severo Ochoa [CBMSO]), Slovenian Research Agency (J3-5506 to B.P.), and Regional Council of Burgundy (PARI 2014). L.C. was supported by a postdoctoral contract from the Centro de Investigación Biomédica en Red de Enfermedades Raras. We thank Barbara Sesé, Luis González-Moreno, David Márquez, and the units of Optical and Confocal Microscopy and Electron Microscopy of the CBMSO for their support.

Received: May 19, 2017
Accepted: September 19, 2017
Published: November 2, 2017

Web Resources

1000 Genomes Project, http://www.1000genomes.org/
ClinVar, https://www.ncbi.nlm.nih.gov/clinvar/
dbSNP Build 141, http://www.ncbi.nlm.nih.gov/projects/SNP/
Genome Aggregation Database (gnomAD), http://gnomad.broadinstitute.org
Modeler 9v14, http://www.salilab.org/modeller/
MutationTaster, http://www.mutationtaster.org/
NAMD 2.11, http://www.ks.uiuc.edu/Research/namd/
OMIM, https://www.omim.org
PolyPhen-2, http://genetics.bwh.harvard.edu/pph2/
Primer3plus, http://www.bioinformatics.nl/cgi-bin/primer3plus/primer3plus.cgi
Program Modeler 9v14, https://salilab.org/modeller/
RSCB Protein Data Bank, https://www.rcsb.org/pdb/home/home.do
SIFT, http://sift.bii.a-star.edu.sg
Visual Molecular Dynamics v.1.9.2, http://www.ks.uiuc.edu/Research/vmd/

References

1. De Sandre-Giovannoli, A., Bernard, R., Cau, P., Navarro, C., Amiel, J., Boccaccio, I., Lyonnet, S., Stewart, C.L., Munnich, A., Le Merrer, M., and Lévy, N. (2003). Lamin a truncation in Hutchinson-Gilford progeria. Science *300*, 2055.
2. Eriksson, M., Brown, W.T., Gordon, L.B., Glynn, M.W., Singer, J., Scott, L., Erdos, M.R., Robbins, C.M., Moses, T.Y., Berglund, P., et al. (2003). Recurrent de novo point mutations in lamin A cause Hutchinson-Gilford progeria syndrome. Nature *423*, 293–298.
3. Marteijn, J.A., Lans, H., Vermeulen, W., and Hoeijmakers, J.H. (2014). Understanding nucleotide excision repair and its roles in cancer and ageing. Nat. Rev. Mol. Cell Biol. *15*, 465–481.
4. Yu, C.E., Oshima, J., Fu, Y.H., Wijsman, E.M., Hisama, F., Alisch, R., Matthews, S., Nakura, J., Miki, T., Ouais, S., et al. (1996). Positional cloning of the Werner's syndrome gene. Science *272*, 258–262.
5. Johnston, J.J., Sanchez-Contreras, M.Y., Keppler-Noreuil, K.M., Sapp, J., Crenshaw, M., Finch, N.A., Cormier-Daire, V., Rademakers, R., Sybert, V.P., and Biesecker, L.G. (2015). A point mutation in PDGFRB causes autosomal-dominant Penttinen syndrome. Am. J. Hum. Genet. *97*, 465–474.

basal membrane potential, we added 6 μM oligomycin to obtain a maximal Δψ and added the protonophore carbonyl cyanide-p-trifluoromethoxyphenylhydrazone (4 μM FCCP) thereafter to fully depolarize mitochondria and obtain a minimal Δψ. Results (TMRM relative fluorescence) are expressed as calibrated basal Δψ calculated as a percentage of the total mitochondrial signal (maximum minus minimal) and correspond to means ± SEM. The significance of the differences between means was evaluated by one-way ANOVA followed by a post hoc Tukey test (***$p < 0.001$, **$p < 0.01$).
(F and G) HeLa cell lines (30×10^3 cells per well) were seeded into Seahorse XF 24 plates for 20 hr, and cellular bioenergetics were analyzed with the Seahorse XF24 Extracellular Flux Analyzer (Seahorse Bioscience).[30–33] Oxygen consumption rates (OCRs) were analyzed under basal conditions in DMEM with 5 mM glucose after the addition of mitochondrial inhibitors: oligomycin (Oligo, 6 μM), 2,4-dinitrophenol (DNP, 0.5 mM), and antimycin A and rotenone (AntA and Rot, 1 μM each) at the indicated time points. (F) OCR traces calculated as the percent change from basal respiration. Data represent the mean ± SEM of four independent experiments. (G) ATP-linked OCR expressed as a percentage of basal mitochondrial respiration. Data represent the mean ± SEM of four independent experiments performed in parallel. Two measurements after the addition of oligomycin from at least 12 independent replicates were used. Results were analyzed by one-way ANOVA followed by a post hoc Tukey test. Comparisons between mutants and WT-1 (a) or WT-2 (b) are indicated (**$p < 0.01$, *$p < 0.05$). No statistical difference was found between the WT and p.Arg217Cys cell lines.
(H and I) Amounts of ATP remained unaffected in HeLa cells expressing p.Arg217Cys SLC25A24. HeLa CRT-1, WT-2, R217C-1, and R217C-2 lines were transfected with the mitochondrial-targeted GO-ATeam2 (mit GO-ATeam2, provided by H. Noji) (H) or the cytosolic GO-ATeam1 (cyt GO-ATeam1, provided by H. Noji) (I) probes, and 48 hr later basal amounts of ATP were determined via measurement of the fluorescence emission ratio (OFP/GFP) as previously described.[30,34] The results correspond to the mean ± SEM from three independent experiments performed in parallel for each line (30–70 cells per experiment). At least 120 cells were analyzed per cell line. The significance of differences between cell lines was analyzed by paired t tests.
(J) Amounts of mitochondrial ATP in CRT-1, WT-2, and R217C-1 cells transfected with mitGO-ATeam2 during the addition of 2 μm oligomycin (Oligo). Changes in ATP amounts were calculated as the normalized ratio (OFP/GFP)/R0 (where R0 is the OFP/GFP ratio before the addition of oligomycin). The results correspond to the mean ± SEM from two to three independent experiments and three to five cells per experiment.

6. Fontaine, G., Farriaux, J.P., Blanckaert, D., and Lefebvre, C. (1977). [A new complex polymalformative syndrome (author's transl)]. J. Genet. Hum. *25*, 109–119.
7. Petty, E.M., Laxova, R., and Wiedemann, H.R. (1990). Previously unrecognized congenital progeroid disorder. Am. J. Med. Genet. *35*, 383–387.
8. Rodríguez, J.I., Pérez-Alonso, P., Funes, R., and Pérez-Rodríguez, J. (1999). Lethal neonatal Hutchinson-Gilford progeria syndrome. Am. J. Med. Genet. *82*, 242–248.
9. Faivre, L., Khau Van Kien, P., Madinier-Chappat, N., Nivelon-Chevallier, A., Beer, F., and LeMerrer, M. (1999). Can Hutchinson-Gilford progeria syndrome be a neonatal condition? Am. J. Med. Genet. *87*, 450–452, author reply 453–454.
10. Heyland, K., Hodler, C., and Baenziger, O. (2003). Yunis-Varon syndrome (Swiss Society of Neonatology). http://www.neonet.ch/files/5314/2054/8445/January_2003.pdf.
11. Delgado-Luengo, W.N., Petty, E.M., Solís-Añez, E., Römel, O., Delgado-Luengo, J., Hernández, M.L., Morales-Machín, A., Borjas-Fuentes, L., Zabala-Fernández, W., González-Ferrer, S., et al. (2009). Petty-Laxova-Wiedemann progeroid syndrome: further phenotypical delineation and confirmation of a rare syndrome of premature aging. Am. J. Med. Genet. A. *149A*, 2200–2205.
12. Castori, M., Silvestri, E., Pedace, L., Marseglia, G., Tempera, A., Antigoni, I., Torricelli, F., Majore, S., and Grammatico, P. (2009). Fontaine-Farriaux syndrome: a recognizable craniosynostosis syndrome with nail, skeletal, abdominal, and central nervous system anomalies. Am. J. Med. Genet. A. *149A*, 2193–2199.
13. Braddock, S.R., Ardinger, H.H., Yang, C.S., Paschal, B.M., and Hall, B.D. (2010). Petty syndrome and Fontaine-Farriaux syndrome: Delineation of a single syndrome. Am. J. Med. Genet. A. *152A*, 1718–1723.
14. del Arco, A., and Satrústegui, J. (2004). Identification of a novel human subfamily of mitochondrial carriers with calcium-binding domains. J. Biol. Chem. *279*, 24701–24713.
15. Fiermonte, G., De Leonardis, F., Todisco, S., Palmieri, L., Lasorsa, F.M., and Palmieri, F. (2004). Identification of the mitochondrial ATP-Mg/Pi transporter. Bacterial expression, reconstitution, functional characterization, and tissue distribution. J. Biol. Chem. *279*, 30722–30730.
16. Palmieri, F. (2013). The mitochondrial transporter family SLC25: identification, properties and physiopathology. Mol. Aspects Med. *34*, 465–484.
17. Aprille, J.R. (1993). Mechanism and regulation of the mitochondrial ATP-Mg/P(i) carrier. J. Bioenerg. Biomembr. *25*, 473–481.
18. Traba, J., Del Arco, A., Duchen, M.R., Szabadkai, G., and Satrústegui, J. (2012). SCaMC-1 promotes cancer cell survival by desensitizing mitochondrial permeability transition via ATP/ADP-mediated matrix Ca(2+) buffering. Cell Death Differ. *19*, 650–660.
19. Bernardi, P., Rasola, A., Forte, M., and Lippe, G. (2015). The Mitochondrial Permeability transition pore: channel formation by F-ATP synthase, integration in signal transduction, and role in pathophysiology. Physiol. Rev. *95*, 1111–1155.
20. Kunji, E.R., and Crichton, P.G. (2010). Mitochondrial carriers function as monomers. Biochim. Biophys. Acta *1797*, 817–831.
21. Palmieri, F. (2014). Mitochondrial transporters of the SLC25 family and associated diseases: a review. J. Inherit. Metab. Dis. *37*, 565–575.
22. Dehez, F., Pebay-Peyroula, E., and Chipot, C. (2008). Binding of ADP in the mitochondrial ADP/ATP carrier is driven by an electrostatic funnel. J. Am. Chem. Soc. *130*, 12725–12733.
23. Wang, Y., and Tajkhorshid, E. (2008). Electrostatic funneling of substrate in mitochondrial inner membrane carriers. Proc. Natl. Acad. Sci. USA *105*, 9598–9603.
24. Sali, A., and Blundell, T.L. (1993). Comparative protein modelling by satisfaction of spatial restraints. J. Mol. Biol. *234*, 779–815.
25. Phillips, J.C., Braun, R., Wang, W., Gumbart, J., Tajkhorshid, E., Villa, E., Chipot, C., Skeel, R.D., Kalé, L., and Schulten, K. (2005). Scalable molecular dynamics with NAMD. J. Comput. Chem. *26*, 1781–1802.
26. Humphrey, W., Dalke, A., and Schulten, K. (1996). VMD: visual molecular dynamics. J. Mol. Graph. *14*, 33–38, 27–28.
27. Pebay-Peyroula, E., Dahout-Gonzalez, C., Kahn, R., Trézéguet, V., Lauquin, G.J., and Brandolin, G. (2003). Structure of mitochondrial ADP/ATP carrier in complex with carboxyatractyloside. Nature *426*, 39–44.
28. van Kuilenburg, A.B., Meijer, J., Mul, A.N., Hennekam, R.C., Hoovers, J.M., de Die-Smulders, C.E., Weber, P., Mori, A.C., Bierau, J., Fowler, B., et al. (2009). Analysis of severely affected patients with dihydropyrimidine dehydrogenase deficiency reveals large intragenic rearrangements of DPYD and a de novo interstitial deletion del(1)(p13.3p21.3). Hum. Genet. *125*, 581–590.
29. Davidson, S.M., Yellon, D., and Duchen, M.R. (2007). Assessing mitochondrial potential, calcium, and redox state in isolated mammalian cells using confocal microscopy. Methods Mol. Biol. *372*, 421–430.
30. Rueda, C.B., Traba, J., Amigo, I., Llorente-Folch, I., González-Sánchez, P., Pardo, B., Esteban, J.A., del Arco, A., and Satrústegui, J. (2015). Mitochondrial ATP-Mg/Pi carrier SCaMC-3/Slc25a23 counteracts PARP-1-dependent fall in mitochondrial ATP caused by excitotoxic insults in neurons. J. Neurosci. *35*, 3566–3581.
31. Qian, W., and Van Houten, B. (2010). Alterations in bioenergetics due to changes in mitochondrial DNA copy number. Methods *51*, 452–457.
32. Llorente-Folch, I., Rueda, C.B., Amigo, I., del Arco, A., Saheki, T., Pardo, B., and Satrústegui, J. (2013). Calcium-regulation of mitochondrial respiration maintains ATP homeostasis and requires ARALAR/AGC1-malate aspartate shuttle in intact cortical neurons. J. Neurosci. *33*, 13957–13971.
33. Brand, M.D., and Nicholls, D.G. (2011). Assessing mitochondrial dysfunction in cells. Biochem. J. *435*, 297–312.
34. Nakano, M., Imamura, H., Nagai, T., and Noji, H. (2011). Ca^{2+} regulation of mitochondrial ATP synthesis visualized at the single cell level. ACS Chem. Biol. *6*, 709–715.
35. Formentini, L., Sánchez-Aragó, M., Sánchez-Cenizo, L., and Cuezva, J.M. (2012). The mitochondrial ATPase inhibitory factor 1 triggers a ROS-mediated retrograde prosurvival and proliferative response. Mol. Cell *45*, 731–742.
36. Warburg, O. (1956). On the origin of cancer cells. Science *123*, 309–314.
37. Rivera-Torres, J., Acín-Perez, R., Cabezas-Sánchez, P., Osorio, F.G., Gonzalez-Gómez, C., Megias, D., Cámara, C., López-Otín, C., Enríquez, J.A., Luque-García, J.L., and Andrés, V. (2013). Identification of mitochondrial dysfunction in Hutchinson-Gilford progeria syndrome through use of stable isotope labeling with amino acids in cell culture. J. Proteomics *91*, 466–477.

38. Peinado, J.R., Quirós, P.M., Pulido, M.R., Mariño, G., Martínez-Chantar, M.L., Vázquez-Martínez, R., Freije, J.M., López-Otín, C., and Malagón, M.M. (2011). Proteomic profiling of adipose tissue from Zmpste24-/- mice, a model of lipodystrophy and premature aging, reveals major changes in mitochondrial function and vimentin processing. Mol. Cell. Proteomics *10*, 008094.
39. Scheibye-Knudsen, M., Ramamoorthy, M., Sykora, P., Maynard, S., Lin, P.C., Minor, R.K., Wilson, D.M., 3rd, Cooper, M., Spencer, R., de Cabo, R., et al. (2012). Cockayne syndrome group B protein prevents the accumulation of damaged mitochondria by promoting mitochondrial autophagy. J. Exp. Med. *209*, 855–869.
40. Shiloh, Y., and Ziv, Y. (2013). The ATM protein kinase: regulating the cellular response to genotoxic stress, and more. Nat. Rev. Mol. Cell Biol. *14*, 197–210.
41. Scheibye-Knudsen, M., Fang, E.F., Croteau, D.L., and Bohr, V.A. (2014). Contribution of defective mitophagy to the neurodegeneration in DNA repair-deficient disorders. Autophagy *10*, 1468–1469.
42. Sieprath, T., Corne, T.D., Nooteboom, M., Grootaert, C., Rajkovic, A., Buysschaert, B., Robijns, J., Broers, J.L., Ramaekers, F.C., Koopman, W.J., et al. (2015). Sustained accumulation of prelamin A and depletion of lamin A/C both cause oxidative stress and mitochondrial dysfunction but induce different cell fates. Nucleus *6*, 236–246.
43. Maynard, S., Fang, E.F., Scheibye-Knudsen, M., Croteau, D.L., and Bohr, V.A. (2015). DNA Damage, DNA Repair, Aging, and Neurodegeneration. Cold Spring Harb. Perspect. Med. *5*, 025130.
44. Palmieri, F., and Monné, M. (2016). Discoveries, metabolic roles and diseases of mitochondrial carriers: A review. Biochim. Biophys. Acta *1863*, 2362–2378.
45. Palmieri, L., Alberio, S., Pisano, I., Lodi, T., Meznaric-Petrusa, M., Zidar, J., Santoro, A., Scarcia, P., Fontanesi, F., Lamantea, E., et al. (2005). Complete loss-of-function of the heart/muscle-specific adenine nucleotide translocator is associated with mitochondrial myopathy and cardiomyopathy. Hum. Mol. Genet. *14*, 3079–3088.
46. Thompson, K., Majd, H., Dallabona, C., Reinson, K., King, M.S., Alston, C.L., He, L., Lodi, T., Jones, S.A., Fattal-Valevski, A., et al. (2016). Recurrent De Novo Dominant Mutations in SLC25A4 Cause Severe Early-Onset Mitochondrial Disease and Loss of Mitochondrial DNA Copy Number. Am. J. Hum. Genet. *99*, 1405.
47. Kaukonen, J., Juselius, J.K., Tiranti, V., Kyttälä, A., Zeviani, M., Comi, G.P., Keränen, S., Peltonen, L., and Suomalainen, A. (2000). Role of adenine nucleotide translocator 1 in mtDNA maintenance. Science *289*, 782–785.
48. Trifunovic, A., Wredenberg, A., Falkenberg, M., Spelbrink, J.N., Rovio, A.T., Bruder, C.E., Bohlooly-Y, M., Gidlöf, S., Oldfors, A., Wibom, R., et al. (2004). Premature ageing in mice expressing defective mitochondrial DNA polymerase. Nature *429*, 417–423.
49. Bailey, L.J., Cluett, T.J., Reyes, A., Prolla, T.A., Poulton, J., Leeuwenburgh, C., and Holt, I.J. (2009). Mice expressing an error-prone DNA polymerase in mitochondria display elevated replication pausing and chromosomal breakage at fragile sites of mitochondrial DNA. Nucleic Acids Res. *37*, 2327–2335.
50. Ahlqvist, K.J., Hämäläinen, R.H., Yatsuga, S., Uutela, M., Terzioglu, M., Götz, A., Forsström, S., Salven, P., Angers-Loustau, A., Kopra, O.H., et al. (2012). Somatic progenitor cell vulnerability to mitochondrial DNA mutagenesis underlies progeroid phenotypes in Polg mutator mice. Cell Metab. *15*, 100–109.
51. Del Arco, A., Contreras, L., Pardo, B., and Satrustegui, J. (2016). Calcium regulation of mitochondrial carriers. Biochim. Biophys. Acta *1863*, 2413–2421.
52. Traba, J., Satrústegui, J., and del Arco, A. (2011). Adenine nucleotide transporters in organelles: novel genes and functions. Cell. Mol. Life Sci. *68*, 1183–1206.
53. Amigo, I., Traba, J., González-Barroso, M.M., Rueda, C.B., Fernández, M., Rial, E., Sánchez, A., Satrústegui, J., and Del Arco, A. (2013). Glucagon regulation of oxidative phosphorylation requires an increase in matrix adenine nucleotide content through Ca2+ activation of the mitochondrial ATP-Mg/Pi carrier SCaMC-3. J. Biol. Chem. *288*, 7791–7802.
54. Anunciado-Koza, R.P., Zhang, J., Ukropec, J., Bajpeyi, S., Koza, R.A., Rogers, R.C., Cefalu, W.T., Mynatt, R.L., and Kozak, L.P. (2011). Inactivation of the mitochondrial carrier SLC25A25 (ATP-Mg2+/Pi transporter) reduces physical endurance and metabolic efficiency in mice. J. Biol. Chem. *286*, 11659–11671.
55. Urano, T., Shiraki, M., Sasaki, N., Ouchi, Y., and Inoue, S. (2015). SLC25A24 as a novel susceptibility gene for low fat mass in humans and mice. J. Clin. Endocrinol. Metab. *100*, E655–E663.
56. Ehmke, N., Graul-Neumann, L., Smorag, L., Koenig, R., Segebrecht, L., Magoulas, P., Scaglia, F., Kilic, E., Hennig, A.F., Adolphs, N., et al. (2017). De Novo Mutations in SLC25A24 Cause a Craniosynostosis Syndrome with Hypertrichosis, Progeroid Appearance, and Mitochondrial Dysfunction. Am. J. Hum. Genet. *101*, this issue, 833–843.